The 7th World Congress on Particle Technology (WCPT7)

In situ deformation and breakage of silica particles inside a SEM

Stefan Romeis, Jonas Paul, Patrick Herre, Mathias Hanisch, Robin N. Klupp Taylor, Jochen Schmidt, and Wolfgang Peukert*

Institute of Particle Technology (LFG), Friedrich-Alexander-Universität Erlangen-Nürnberg, Cauerstraße 4, 91058 Erlangen, Germany

Abstract

Mechanical properties and particle breakage behavior in the submicron size range are of fundamental importance for many particle related processes and applications. Although many (in situ) studies have been dedicated to materials' size dependent mechanical characterization, particles as free standing structures have been omitted widely. An important, yet open question is the structure property relationship at small scales. Within this account, the application of a custom built manipulator for particle compression inside a scanning electron microscope (SEM) is presented: Stöber-Fink-Bohn (SFB) particles with mean diameters of 500 nm and 1000 nm are subjected to heat treatments and their mechanical properties are directly correlated to the internal structure. The as-synthesized SFB particles exhibit a complex and size dependent internal structure. Mechanical properties undermatching the values of fused silica are found and only plastic cracking at large strains is observed: cracks are formed at the surface and propagate in radial direction towards the particle center. Heat treatment leads to densification. The degree of changes is controlled by temperature and treatment time. Starting from initially low values, Young's modulus and hardness are increasing with treatment temperature. Properties of fused silica are approached or even exceeded after a treatment at 1000°C. A significant level of plasticity and high sustained deformations are still found. Whereas small particle show ductile cracking, the heat treated micron sized particles show a brittle behavior. A brittle to ductile transition in the size range of 500 nm to 1000 nm is thus identified.

* Corresponding author. Tel.: +49 (0)9131 85-29401; fax: +49 (0)9131 85-29402.
  E-mail address: Wolfgang.peukert@fau.de

1. Introduction

Mechanical properties on the submicron to nanometer scale are crucial for various applications of particulate systems, including microelectronics, sensors, powder flow, ceramic manufacturing, and tableting. Despite their obvious importance to design suitable long living products, the mechanical responses of small structures and especially particulate systems to applied external loads are poorly understood. The main reason is found in the encountered experimental difficulties: localizing the position of the small structures, application of a well-defined stress, measuring small forces (<100 μN) and deformations (~nm), and the correct interpretation of the recorded force displacement data. Problems of positioning and alignment and data interpretation can be overcome (at least partially) using in situ scanning electron microscopy (SEM) and transmission electron microscopy (TEM) techniques: for electron transparent samples TEM allows the direct observation of the microstructure, but inherently suffer from a highly limited space in between the pole gap pieces; information obtained from SEM techniques is limited to surface near areas, but the higher working distance and the generally larger space in the vacuum chamber impose much less design constraints on the in situ apparatus: actuators and sensors can be completely integrated, limiting the required through-puts from outside the vacuum chamber to signal- and controlling-wires. Over the past years, various in situ devices (see e.g. [1-8]) have been integrated into scanning electron microscopes, whereby the first straining stages were mechanically driven from outside the SEM. Today, even first commercial solutions for both SEM and TEM exist [6; 9-11]. For further details on the history and recent developments of electron microscopy based in situ testing devices see Legros et al. [12] and the references given in Romeis et al. [13] and Paul et al. [14].

Here we report on a recently developed in situ manipulator for mechanical characterization of colloidal particles in a high resolution field emission scanning electron microscope and its application to investigate the mechanical behavior spherical Stöber Fink Bohn (SFB) particles [13-16]. Contrasting existing concepts our device covers a wide measuring range by a simple adjustment of the spring based force sensor and a force resolution < 100 nN accompanied by an accuracy in deformation measurement of about 5 nm can be achieved.

2. Custom built in situ SEM manipulator and data evaluation
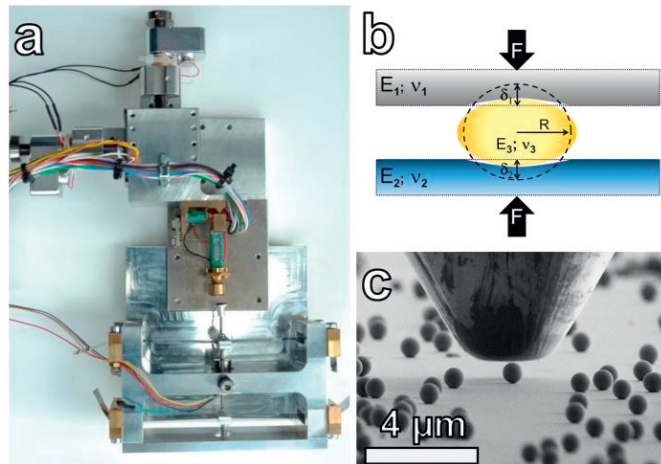
2.1. Custom built SEM manipulator

Fig. 1. (a) Custom built SEM manipulator, (b) schematics of the contact zone (c) SEM image prior to stressing of a single particle.

A custom-built manipulation device integrated in a high resolution scanning electron microscope was used [13] to stress single submicron particles. A photographic image of the device is shown in Fig. 1 (a). Basically, two

assembly units can be distinguished, i.e. an upper part termed "Nanomanipulator" and a lower part called "Load Cell". The Nanomanipulator is comprised of a two dimensional coarse positioning stage (Newport, USA) and an attached piezoelectric tripod scanner equipped with strain gauges (Anfatec Instruments AG, Germany). All movements of the employed diamond flat punch indenter (Synton-MDP, Switzerland, plateau diameter 3 µm, rms roughness 0.4 nm) are realized by the Nanomanipulator: the 2-dimensional positioning stage allows for coarse positioning and for approaching the sample surface; the tripod scanner is used for fine positioning and performs tip movements during particle stressing. The sample supporting Load Cell acts as force sensor: two interlocked leaf foils supporting the sample are deflected by the applied forces. The deflection is measured by a linear variable differential transformer. With the spring stiffness being calculated from Eigenfrequency, acting forces can be derived. Particle deformation is obtained as the difference of tripod scanner elongation and deflection of the spring system. As can be seen in Fig. 1 (c) proper imaging is achieved by tilting the whole device at an appropriate working distance (approx. 7 mm) by 4° with respect to the primary electron beam.

Particles were stressed continuously with a fixed probe displacement rate (200 nm/s) to different final loads. Due to the apparatus design and the particle deformation behavior, actual loading rates differ; by a separate set of experiments (data not shown) rate influences were excluded in the working range. Influences of the electron beam on the deformation behavior have been reported especially for silica materials [13; 14; 17]. Thus, we used low energy conditions for imaging leaving the samples unchanged [14], and the electron beam was blanked during the mechanical tests completely.

2.2. Evaluation of force deformation data

The loading part of the recorded force deformation data consists of an elastic part followed by a linear elastic-plastic and a nonlinear elastic-plastic regime. At higher strains discontinuities associated with crack formation [13] or the full fragmentation of the particle occurs. Applied methods to retrieve Young's modulus (E), CEB hardness (H_{CEB}), the elastic-plastic loading index (EPL), and the volume specific energy dissipated during cracking ($E_{v,diss}$) are described by Paul et al. [14]. Briefly, elastic properties were obtained by Hertzian fitting to the elastic deformation regime [18]; the upper limit of the elastic regime was determined by compression of several particles only in the elastic range as indicated by SEM imaging and coinciding force-displacement data. The CEB model [19] was applied to the linear elastic-plastic regime to obtain a measure for particle hardness. The EPL index [20] is a measure of plasticity at a given strain: the energy spent during loading and the recovered energy during unloading are compared (both obtained by integration of force displacement data). The energy dissipated during cracking is obtained from the difference in volume specific energy prior- and after the discontinuity observed in the force-displacement data. Volume specific energy is obtained by integration of the respective force deformation data and subsequent normalization to the initial particle volume. For data evaluation the following simplifying assumptions were made (load situation is schematically depicted in Fig. 1 (b)): total deformation is evenly distributed between both contacts pair, i.e. probe / sample and sample / substrate; bulk Poisson ratios and Young's moduli for silica ($\nu = 0.17$), diamond ($\nu = 0.07$; E = 1143 GPa), and silicon ($\nu = 0.22$; E = 130 GPa) are used. Particle radii are obtained by SEM imaging. The consistent application of the described models enables the comparison of the mechanical behavior for the different samples.

2.3. Sample preparation for in-situ SEM manipulator

To avoid hydroxylation and the formation of solid bridges due to precipitation of dissolved silica, the samples for the single particle compression experiments were prepared completely solvent free: SFB particles were individualized and spread on small rectangular pieces (5 x 5 mm²) of a (100) silicon wafer by placing tiny amounts of the dry powders onto the surface and subsequent rubbing against a second wafer piece. The resulting particle distribution is of course random.

3. Experimental

3.1. SFB silica and heat treatment

SFB silica samples with nominal diameters of 500 nm and 1000 nm, were recovered from solution by centrifugation (3-30KS Sigma Laborzentrifugen, Germany, 15 min, 65403 g, 20±5°C) followed by overnight drying in an oven (Function Line, Heraeus, 70 °C). The powders were subjected to heat treatments in a furnace (LE 6/11, Nabatherm, Germany): In a first set of experiments 500 nm SFB particles were treated for 12h at 400°C, 800°C, and 1000°C. In a second set of experiments 1000 nm particles were treated at 1000°C for 12h, 24h, and 36h.

3.2. Scanning electron microscopy (Ultra FE-SEM Gemini Ultra 55, Carl Zeiss, Germany)

Accelerating voltage was 2 kV; the final aperture was 10 µm; working distance accounted for approx. 4 mm. Secondary electrons were used for imaging. To obtain mean particle sizes images were converted to binary images and projected areas were determined. Over 500 particles were evaluated for each sample.

3.3. Raman spectroscopy (LabRAM HR – Evolution, Horiba Scientific Ltd., USA)

A micro Raman setup was used. Grating, slit and hole were 1800 gr/mm, 100 µm and 1200 µm. Spectra where collected for Raman shifts of 100 cm^{-1} to 1200 cm^{-1} with an acquisition time of 60 s. Spectral resolution was 1 cm^{-1}. The presented data is smoothed (Savitzky-Golay, 10-points), base line corrected, and was normalized to the band at 800 cm^{-1}.

3.4. Infrared spectroscopy (FTS 3100 Spectrometer, Varian, USA)

IR transmission spectra were recorded in the spectral range from 3800 cm^{-1} to 400 cm^{-1}. Resolution was 2 cm^{-1}. For measurement, samples were dispersed (1/1000 m/m) in KBr (UVASol, for IR spectroscopy, Merck KGaA, Germany). Base line corrections were performed manually; data is normalized to maximum absorbance.

4. Results and discussion

4.1. Structural changes during thermal treatment

In a first set of experiments the influence of treatment temperature at constant heating time was investigated for 500 nm SFB particles. In course of the thermal treatments we find significant changes in porosity, density, and the internal particle structure. Table 1 lists the mean particle sizes $x_{50,3}$, mass specific geometric surface S_m areas obtained from SEM imaging, and the powder densities obtained by helium pycnometry. A smoothing of the particles over the heating is evident from the SEM imaging (data not shown).

Table 1. Mean particle size, geometric surface areas, and powder densities for 500 nm SFB.

	70°C	400°C	800°C	1000°C
Mean particle size $x_{50,3}$ / nm	480	474	454	443
Mass specific geometric surface area S_m m²/g	5.7	5.7	5.9	6.2
Powder density ρ / g/cm³	1.91	2.06	2.24	2.24

From the data presented in Table 1 enhanced cross linking and structural densification in course of the thermal treatment can be assumed. Further insight into structural changes is gained by vibrational spectroscopy: Fig. 2 displays Raman (A) and infrared (B) spectra obtained for the different samples.
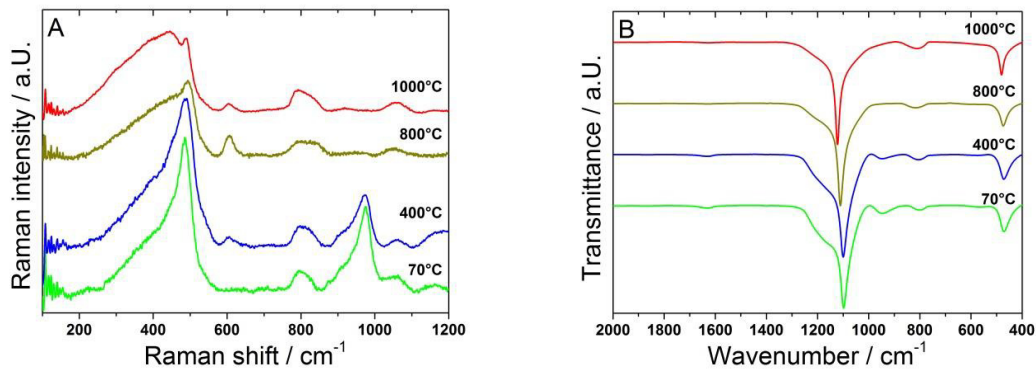
Fig. 2. Left: Raman spectra of the 500 nm SFB samples treated at different temperatures Right: Corresponding IR spectra for the samples.

In the Raman spectra (Fig. 2 A) the disappearance of the band at 973 cm^{-1} after a heat treatment at 800°C is most obvious. This mode is assigned to Si-OH stretching [21], i.e. upon heating SiOH groups are removed and condensation to Si-O-Si bonds occurs. The shift of the band initially found at 430 cm^{-1} (untreated) to 440 cm^{-1} (1000°C) is in good accordance: the band is assigned to the symmetric stretching mode ν_s of the Si-O-Si bonds and its exact position depends on bond angle as well as the Si-O bond length [22]. It can thus be concluded that the arrangement of the SiO$_4$ units changes in course of the heat treatment. The bands at 478 cm^{-1} (untreated) / 488 cm^{-1} (heat treated) and 604 cm^{-1} (heat treated sample) can be assigned to the D$_1$ and D$_2$ band, i.e. to planar 4-fold and 3-fold Si-O rings[22; 23]. Interestingly, the amount and the arrangement of the 4-fold and 3-fold ring structures dependent on calcination temperature, i.e. the highest relative amount of ring structures is found after the treatment at 800°C. Similar conclusions can be drawn from infrared spectra (Fig. 2 B): four prominent bands involving silicon are found in the wavelength region from 1300 cm^{-1} to 400 cm^{-1}: A rocking mode is observed near 470 cm^{-1} for untreated SFB. This band shifts with increasing treatment temperature to slightly higher wavenumbers. A second feature appears at 800 cm^{-1} and is attributed to Si-O (symmetric) stretching in a O-Si-O bridge within the solid [24]. This feature is unaffected by the thermal treatment. A third band being centered around 945 cm^{-1} (only observed till 400°C) is associated with the stretching of Si-OH surface groups (to our understanding both external and internal surfaces) [24]. The band near 1080 cm^{-1} (untreated silica) is assigned to different asymmetric stretching vibrations of Si-O-Si. The exact position of the corresponding band depends on the oxygen content and the connectivity of the comprising silica units. Thus, the band is most likely a superposition of different vibrations. The shoulder near 1200 cm^{-1} (decreasing with calcination temperature) is associated with the disorder-induced coupling e.g. internal surfaces or reduced cross-linking [25]. Especially the changes of the IR features occurring at 945 cm^{-1}, 1080 cm^{-1}, and 1200 cm^{-1} reflect the densification and increasing cross-linking with treatment temperature. All samples were found X-ray amorphous (data not shown).

4.2. Mechanical properties of thermally treated particles

As can be seen in Fig. 3, the observed changes in mechanical data are in excellent agreement: an increase in Young's modulus and CEB hardness are observed if temperatures of 400°C are exceeded during the thermal treatment.
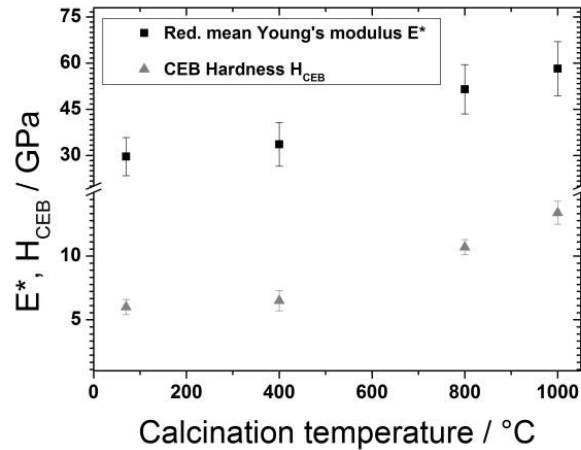
Fig. 3. Mean values of reduced Young's modulus E* and CEB hardness for the 500 nm SFB samples calcinated at different temperatures.

Whereas Young's modulus approaches the bulk value for fused silica (after the thermal treatment at 1000°C we found (71.8±8.6) GPa), CEB hardness is found to even exceed typical bulk values (9-10 GPa). After the heat treatments, still high strains are needed (0.48±0.04) to initiate crack formation and thus spheres of high strength have been obtained. In EPL index - depicted in Fig. 4 for the different samples - we do not find significant changes. It can thus be stated that the overall ductile deformation behaviour is maintained over heat treatment. The sharp kink observed at a strain of approx. 0.5 is most likely caused cracking of the particles. Only the formation of plastic cracks was observed and especially fragmentation into at least two separate pieces has not been observed.
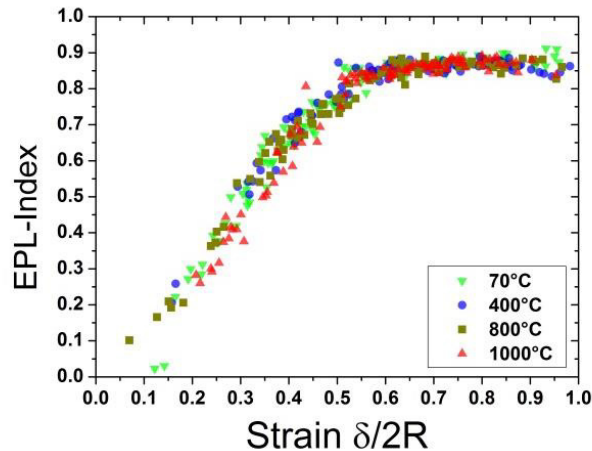

Fig. 4. EPL index of the 500 nm SFB samples deformed to different strain levels.

4.3. Size dependent cracking behavior

In a second set of experiments the size dependency of the mechanical behavior was investigated. To this end, SBF particles with a mean diameter of 1000 nm were heat treated at 1000°C. Judging on basis of the measured mean reduced Young's modulus, lowered mechanical properties compared to fused silica are still found after 12h of heat

treatment. After an extended treatment time of 36h comparable values are found and from vibrational spectroscopy (data not shown) no difference between the 500 nm and 1000 nm silica particles is found anymore. Mean reduced Young's modulus and CEB hardness are given in Fig. 5 for the different heating times. We assume that incomplete densification and insufficient structural relaxation are responsible for this behavior.
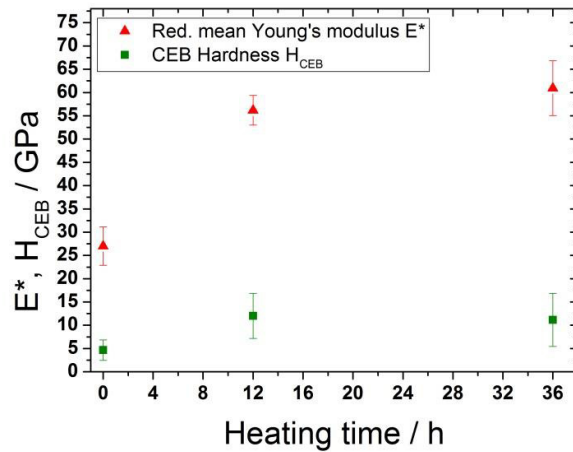
Fig. 5. Mean values of reduced Young's modulus E* and CEB hardness for 1000 nm SFB samples calcinated at 1000°C for different times.

Contrary to the observations made for the 500 nm particles an increase in brittleness is found over the heat treatment of the 1000nm particles: as shown in Fig. 6, the EPL index curves shift to lower values in course of the calcination; again, the sharp kinks in the curves are attributed to crack formation in the particles.
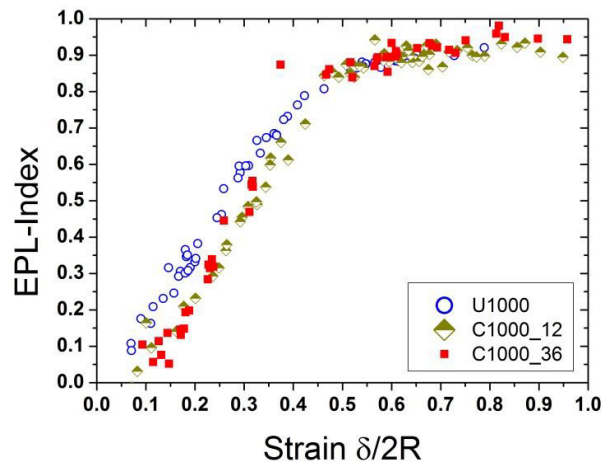
Fig. 6. EPL index for calcined 1000 nm samples deformed to different final strain levels U1000: untreated particles; C1000_12h: 12h calcinated at 1000°C; C1000_36: 36h calcinated at 1000°C.

Interestingly, we also found severe changes in the cracking behavior of the 1000 nm particles: after the heat treatment all particles showed fragmentation into two or more separate pieces. Especially the latter cracking process is accompanied by a high energy release. On basis of the released energy during cracking and the strain at crack

onset, two fragmentation modes, i.e. fragmentation into two pieces and an even more brittle fragmentation into several pieces, can be distinguished. This is clearly seen from Fig. 7. By plotting the energy dissipated during cracking versus the strain at crack onset, the different behaviors can be easily separated: almost independent of the heat treatment (only a slight shift is observable), the smaller 500 nm particles show cracking at high strains with comparatively little energy dissipation; ductile cracks are formed and do not separate the particles into separate pieces.
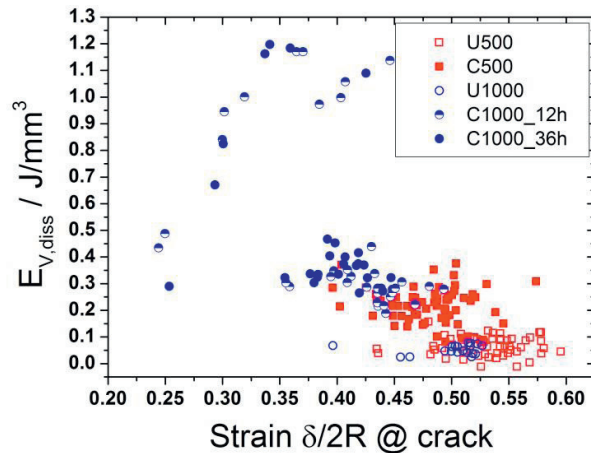

Fig. 7. Released energy at cracking versus strain at onset of crack; U500: untreated 500 nm particles; C500: calcinated 500 nm particles. U1000: untreated 1000 nm particles; C1000_12h: 12h calcinated 1000 nm particles at 1000°C; C1000_36: 1000 nm particles calcinated for 36h at 1000°C.

The behavior of the untreated 1000 nm particles is in perfect agreement; only ductile cracking at high strains occurs. During heat treatment, however, a stronger shift to lower strains and higher dissipated energies is observed, whereby two classes, i.e. fragmentation into two pieces and full fragmentation into several pieces can be clearly distinguished. We associate the cracking at lowest strains with (surface) flaw controlled brittle cracking of the glassy spheres. Hence, a brittle to ductile transition occurs in the size range of 500 nm to 1000 nm; this is in agreement with predictions of Schönert et al. [26] and Kendall et al. [27]. SEM images of the observed cracking modes are shown in Fig. 8.
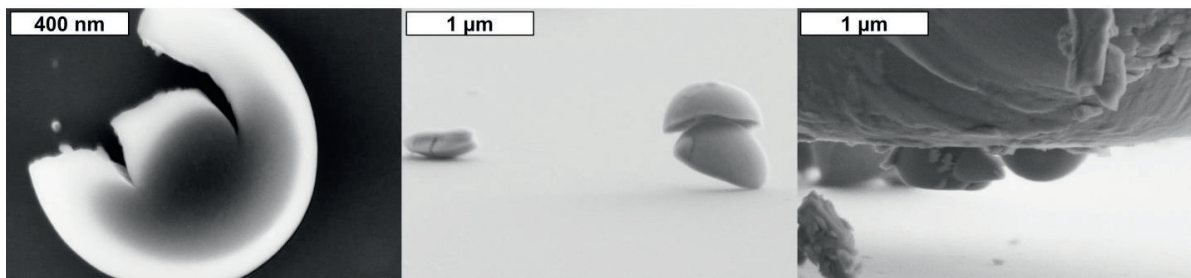

Fig. 8. Different fragmentation modes for 1000 nm SFB particles: untreated particles (left), heat treated particles middle (12h) and right (36h)

5. Conclusion

Within this account, the application of a custom-built SEM supported force sensing manipulator to investigate the mechanical behavior of spherical silica particles was shown. By comparison with vitreous silica, we found significantly reduced mechanical properties in terms of hardness and Young's modulus for the as synthesized material - a behavior well explained by the weakly linked, low density silica network of the particles. Upon thermal treatment, cross-linking is significantly increased and a densification of the particles is found. As a consequence, mechanical properties are enhanced: Young's modulus approaches a typically observed value for bulk fused silica. CEB hardness and sustained strain at cracking or fragmentation of the particles were found to be enhanced with respect to vitreous silica. Silica glass spheres of high strength are thus obtained; this behavior is clearly associated with the micron scale. Cracking behavior after calcination was found to be clearly size dependent: particles with the mean diameter of 500 nm failed only by the formation of ductile cracks and no fragmentation occurred: the cracks are formed at the edge of the contact zones due to peripheral tensile stresses and are driven towards the particle center. A similar behavior was found for larger particles only in the untreated state; after calcination, full fragmentation into at least two pieces occurred. Furthermore, a significant amount of the heat treated 1000 nm silica particles exhibited brittle fracture into several pieces, indicating a brittle to ductile transition in the investigated size range.

Acknowledgements

References

[1] D. Dingley, A simple straining stage for the scanning electron microscope. Micron 1 (1969), pp. 206–210.
[2] H. Bangert, A. Wagendristel, H. Aschinger, Ultramicrohardness tester for use in a scanning electron-microscope. Colloid. Polym. Sci. 259 (1981), pp. 238–240.
[3] H. Bangert, A. Wagendristel, H. Aschinger, Ultra microhardness-measurements on thin-films, fibers and finely structured surfaces. Vakuum-Tech. 31 (1982), pp. 200–203.
[4] R. Rabe, J.-M. Breguet, P. Schwaller, S. Stauss, F. J. Haug, J. Patscheider, J. Michler, Observation of fracture and plastic deformation during indentation and scratching inside the scanning electron microscope. Acta Metall. 469-470 (2004), pp. 206–213.
[5] B. Moser, J. Kuebler, H. Meinhard, W. Muster, J. Michler, Observation of Instabilities during Plastic Deformation by in-situ SEM Indentation Experiments. Adv. Eng. Mater 7 (2005), pp. 388–392.
[6] R. Ghisleni, K. A. Rzepiejewska-Malyska, L. Philippe, P. Schwaller, J. Michler, In Situ SEM Indentation Experiments: Instruments, Methodology, and Applications. Microsc. Res. Tech. 72 (2009), pp. 242–249.
[7] H. Huang, H. Zhao, J. Mi, J. Yang, S. Wan, L. Xu, Z. Ma, A novel and compact nanoindentation device for in situ nanoindentation tests inside the scanning electron microscope. AIP. Advances. 2 (2012), p. 12104.
[8] T. Motoki, W. Gao, S. Kiyono, T. Ono, A nanoindentation instrument for mechanical property measurement of 3D micro/nano-structured surfaces. Meas. Sci. Technol. 17 (2006), pp. 495–499.
[9] D. S. Gianola, A. Sedlmayr, R. Moenig, C. A. Volkert, R. C. Major, E. Cyrankowski, S. A. S. Asif, O. L. Warren, O. Kraft, In situ nanomechanical testing in focused ion beam and scanning electron microscopes. Rev. Sci. Instrum 82 (2011), p. 63901.
[10] K. A. Rzepiejewska-Malyska, G. Buerki, J. Michler, R. C. Major, E. Cyrankowski, S. A. S. Asif, O. L. Warren, In situ mechanical observations during nanoindentation inside a high-resolution scanning electron microscope. J. Mater. Res 23 (2008), pp. 1973–1979.
[11] K. A. Rzepiejewska-Malyska, W. M. Mook, M. Parlinska-Wojtan, J. Hejduk, J. Michler, In situ scanning electron microscopy indentation studies on multilayer nitride films: Methodology and deformation mechanisms. J. Mater. Res 24 (2009), pp. 1208–1221.
[12] R. Legros, D. S. Gianola, C. Motz, Quantitative In Situ Mechanical Testing in Electron Microscopes. MRS Bull 35 (2010), pp. 354–360.
[13] S. Romeis, J. Paul, M. Ziener, W. Peukert, A novel apparatus for in situ compression of submicron structures and particles in a high resolution SEM. Rev. Sci. Instrum 83 (2012), p. 95105.

[14] J. Paul, S. Romeis, J. Tomas, W. Peukert, A review of models for single particle compression and their application to silica microspheres. Adv. Powder. Technol. 25 (2014), pp. 136–153.

[15] W. Stöber, A. Fink, E. Bohn, Controlled growth of monodisperse silica spheres in the micron size range. J. Colloid Interf. Sci. 26 (1968), pp. 62–69.

[16] S. Romeis, J. Paul, M. Hanisch, V. R. R. Marthala, M. Hartmann, R. N. Klupp Taylor, J. Schmidt, W. Peukert, Correlation of Enhanced Strength and Internal Structure for Heat-Treated Submicron Stöber Silica Particles. Part. Part. Syst. Charact (2014), pp. n/a.

[17] K. Zheng, C. Wang, Y. Q. Cheng, Y. Yue, X. Han, Z. Zhang, Z. Shan, S. X. Mao, M. Ye, Y. Yin, E. Ma, Electron-beam-assisted superplastic shaping of nanoscale amorphous silica. Nat. Commun. 1 (2010), pp. 1–8.

[18] H. Hertz, Über die Berührung fester elastischer Körper. J. Reine Angew. Math. 92 (1882), pp. 156–171.

[19] W. R. Chang, I. Etsion, D. B. Bogy, An Elastic-Plastic Model for the Contact of Rough Surfaces. J. Tribol 109 (1987), p. 257.

[20] I. Etsion, Y. Kligerman, Y. Kadin, Unloading of an elastic–plastic loaded spherical contact. Int. J. Solids Struct. 42 (2005), pp. 3716–3729.

[21] P. McMillan, R. L. Remmele, Hydroxyl sites in SiO2 glass; a note on infrared and Raman spectra. Amercian Mineralogist (1986), pp. 772–778.

[22] S. K. Sharma, J. F. Mammone, M. F. Nicol, Raman investigation of ring configurations in vitreous silica. Nature 292 (1981), pp. 140–141.

[23] F. Galeener, Planar rings in glasses. Solid State Communications 44 (1982), pp. 1037–1040.

[24] T. Takamura, H. Yoshida, K. Inazuka, Infrared characteristic bands of highly dispersed silica. Kolloid Z. Z. Polym. 195 (1964), pp. 12–16.

[25] E. I. Kamitsos, A. P. Patsis, G. Kordas, Infrared-reflectance spectra of heat-treated sol-gel-derived silica. Phys. Rev. B 48 (1993), pp. 12499–12505.

[26] K. Schönert, K. Steier, Die Grenze der Zerkleinerung bei kleinen Korngrößen. Chemie Ing. Techn 43 (1971), pp. 773–777.

[27] K. Kendall, The impossibility of comminuting small particles by compression. Nature 272 (1978), pp. 710–711.